Global analysis of the controls on seawater dimethylsulfide spatial variability

George Manville[1,2,3], Thomas G. Bell[2], Jane P. Mulcahy[3], Rafel Simó[4], Martí Galí[4,5], Anoop S. Mahajan[6], Shrivardhan Hulswar[6], Paul R. Halloran[1]

[1]Faculty of Environment, Science and Economy, University of Exeter, Exeter, EX4 4PY, UK
[2]Plymouth Marine Laboratory (PML), Plymouth, PL1 3DH, UK
[3]Met Office, Exeter, EX1 3PB, UK
[4]Institut de Ciències del Mar (ICM-CSIC), Barcelona, 08003, Catalonia, Spain
[5]Barcelona Supercomputing Center (BSC-CNS), Barcelona, 08034, Catalonia, Spain
[6]Indian Institute of Tropical Meteorology (IITM), Ministry of Earth Sciences, Pune, 411008, India

Correspondence to: George Manville (gm441@exeter.ac.uk) and Thomas G. Bell (tbe@pml.ac.uk)

Abstract. Dimethylsulfide (DMS) emitted from the ocean makes a significant global contribution to natural marine aerosol and cloud condensation nuclei, and therefore our planet's climate. Oceanic DMS concentrations show large spatiotemporal variability, but observations are sparse, so products describing global DMS distribution rely on interpolation or modelling. Understanding the mechanisms driving DMS variability, especially at local scales, is required to reduce uncertainty in large scale DMS estimates. We present a study of mesoscale and sub-mesoscale (<100 km) seawater DMS variability that takes advantage of the recent expansion in high frequency seawater DMS observations and uses all available data to investigate the typical distances over which DMS varies in all major ocean basins. These DMS spatial variability lengthscales (VLS) are uncorrelated with DMS concentrations. DMS concentrations and VLS can therefore be used separately to help identify mechanisms underpinning DMS variability. When data are grouped by sampling campaigns, almost 80% of the DMS VLS can be explained using the VLS of sea surface height anomalies, density, and chlorophyll-*a*. Our global analysis suggests that both physical and biogeochemical processes play an equally important role in controlling DMS variability, in contrast with previous results based on data from the low–mid latitudes. The explanatory power of sea surface height anomalies indicates the importance of mesoscale eddies in driving DMS variability, previously unrecognised at a global scale and in agreement with recent regional studies. DMS VLS differs regionally, including surprisingly high frequency variability in low latitude waters. Our results independently confirm that relationships used in the literature to parameterise DMS at large scales appear to be considering the right variables. However, regional DMS VLS contrasts highlight that important driving mechanisms remain elusive. The role of sub-mesoscale features should be resolved or accounted for in DMS process models and parameterisations. Future attempts to map DMS distributions should consider the length scale of variability.

1 Introduction

Dimethylsulfide (DMS) is a volatile sulfur gas produced by surface ocean microbial food webs and emitted to the atmosphere (Bates et al., 1992). DMS emissions dominate atmospheric biogenic sulfur and form a significant component of natural marine aerosol loads (Quinn et al., 2017; Sanchez et al., 2018; Simó, 2001). Aerosols increase light scattering and modify cloud optical properties, thereby contributing to a radiative forcing of climate (Carslaw et al., 2013; Charlson et al., 1987; Galí et al., 2021). The amount, composition, and distribution of natural aerosol in the atmosphere determines the indirect radiative forcing effect of anthropogenic aerosols on climate but is poorly constrained by global climate models (Carslaw et al., 2013). DMS derived sulfate aerosols are ephemeral (~1 day residence time Boucher et al., 2003) and of greater consequence for cloud modulation in remote pristine regions (Halloran et al., 2010). The distribution of natural marine aerosol sources should be represented at the resolution required to capture the frequency and magnitude of their variability. This is critical for reducing the large uncertainties associated with natural aerosol-cloud interactions.

Oceanic DMS production and consumption pathways are complex, and the controls on DMS spatial distribution in the global ocean are not fully resolved (Galí & Simó, 2015). The global surface seawater DMS database contains measurements that show large scale temporal and spatial variability in DMS concentrations (Hulswar et al., 2022; Lana et al., 2011). *In-situ* DMS measurements are relatively sparse and limited with respect to global distribution, coverage, and spatiotemporal sampling frequency, which renders the majority of DMS observations insufficient to resolve local and sub-mesoscale variability (Belviso, Moulin, et al., 2004; Lana et al., 2011; Tortell et al., 2011). DMS sampling is globally biased towards spring-summer months (see Fig. S1, Supplementary Material) and has disproportionally targeted biologically productive areas (e.g., northeast Pacific and northwest Atlantic, see Fig. 1), which can lead to an overrepresentation of high DMS concentrations within the database (Galí et al., 2018). Monthly and repeat interannual DMS measurements are rare, and generally restricted to DMS productive areas (Galí et al., 2018; Tesdal et al., 2015). Sparse, infrequent, and seasonally/spatially biased observations of highly variable DMS concentrations create uncertainty because it is hard to quantify the representativeness of the measurements. Sampling uncertainties inevitably propagate through to DMS concentration and flux climatologies, parameterisations, and model outputs (Belviso et al., 2004).

Relatively simple extrapolation methods have been used to fill the gaps between sparse observations to provide globally representative estimates of DMS (Hulswar et al., 2022; Kettle et al., 1999; Lana et al., 2011). Significant differences in these smoothed climatological estimates, and thus uncertainties, have been attributed to the gap filling techniques used, specifically the appropriate interpolation/smoothing radius of influence (Hulswar et al., 2022). More complex algorithms have been generated at the basin or global scale using parameters such as chlorophyll, light, nutrients, surface temperature, and mixed layer depth (Anderson et al., 2001; Aranami & Tsunogai, 2004; Aumont et al., 2002; Belviso, Moulin, et al., 2004; Chu et al., 2003; Galí et al., 2015, 2018; Halloran et al., 2010; Herr et al., 2019; Miles et al., 2009; Simó & Dachs, 2002; Vallina & Simó,

2007). More recently, global and regional climatologies have been generated using machine learning approaches (Humphries et al., 2012; McNabb & Tortell, 2022, 2023; Wang et al., 2020). The variation in different climatological DMS estimates highlights that the scientific community needs to better understand and map the processes controlling its oceanic distribution (Belviso et al., 2004; Halloran et al., 2010). Modelled seasonal/regional aerosol-cloud interactions and radiative forcing are directly sensitive to the accuracy/choice of seawater DMS estimates (Mahajan et al., 2015; Woodhouse et al., 2010, 2013).

Recent studies have focussed on local and sub-mesoscale DMS variability, taking advantage of improvements to seawater DMS concentration sampling resolution (e.g., Asher et al., 2011; Nemcek et al., 2008; Tortell, 2005a, 2005b; Tortell & Long, 2009; Zindler et al., 2014). This study explores the potential mechanisms that appear to govern DMS variability at the <100 km scale and investigates whether these align with the variables used within large scale DMS parameterisations. An improved understanding of sub-mesoscale DMS variability will aid the development of future climatological flux estimates and the appropriate radius of influence that sparse observations should be afforded when smoothing and interpolating in situ observations.

Variability lengthscale (VLS) analysis is a powerful tool for quantifying sub-mesoscale variability. VLS analysis can be used to indicate the lowest sampling resolution necessary to capture most of the spatial variability (Royer et al., 2015). High resolution measurements are required to assess small scale variability. For example, to observe variations within 10 km when the research ship is travelling at 8 m s^{-1} requires measurements every 20 mins. Instruments that can observe variability at these high resolutions have been deployed in recent years and have contributed substantially to the global DMS database (Hulswar et al., 2022). A growing number of high frequency DMS measurements offers the opportunity for a global analysis of the drivers of DMS variability at small scales.

VLS analysis for DMS has been applied in only a few studies, with most focusing on a specific region and/or a single sampling campaign (e.g., Ross Sea; (Tortell et al., 2011; Tortell & Long, 2009), northeast subarctic Pacific (Asher et al., 2011; Nemcek et al., 2008; Tortell, 2005b)). A larger scale VLS analysis was undertaken on the 7-month low–mid latitude global circumnavigation conducted during the Malaspina Expedition 2010 (Royer et al., 2015). Royer et al. (2015) combined their VLS analysis with VLS values from 3 high latitude studies (7–15 km, Asher et al., 2011; Nemcek et al., 2008; Tortell et al., 2011) and reported an inverse relationship between DMS VLS and latitude (R = –0.74, p < 0.005). Royer et al. (2015) also reported that biological variables dominate over physical variables as drivers of DMS VLS in low latitude regions. While it is tempting to draw global conclusions from the similarities and differences between these studies, each study adopts a slightly different approach to the data treatment, measurement of interpolation error, and/or classification of VLS (see Table S1, Supplementary Material).

This study applies a single, objective VLS analysis to high frequency global DMS observations over the past 15 years (Fig. 1 & S1). The dataset used includes all available data from previous VLS studies. Our study assesses whether the factors controlling DMS variability can be identified using a sub-mesoscale variability analysis across all ocean basins. Sect. 2 describes the datasets used and the VLS methodology. Sect. 3 presents results including global VLS statistics, regional patterns of DMS variability, and drivers of DMS variability. Finally, the findings are discussed in Sect. 4, with conclusions made in Sect. 5.

2 Data & methods

2.1 Seawater DMS data

The majority of DMS data are sourced from the global surface seawater DMS database (GSSDD; see https://saga.pmel.noaa.gov/dms/). Selection criteria are used to identify datasets suitable for sub-mesoscale VLS analysis: a minimum of 100 data points in total and ≤1 hour between measurements, which excludes all data with a spatial resolution >30 km. Applying these filters results in 37 eligible datasets (collected between 2004 and 2019). The filters broadly separate the DMS database by sampling method, highlighting the rapid shift during the early 2000's from discrete, low frequency gas chromatography analytical systems, to continuous, semi-automated high frequency mass spectrometry (Bell et al., 2012; Saltzman et al., 2009). Additional data are from the Malaspina Expedition in 2010-2011 (M10, Royer et al., 2015), the North Atlantic Aerosol and Marine Ecosystem Study in 2015–2018 (NAAMES; Bell et al., 2021; Fig. 1 & S1, Table S2, campaign numbers: 33 (blue), 34 (green), 35 (red), 36 (yellow)), and the Southern oCean SeAsonaL Experiment in 2019 (SCALE; Manville et al. In Prep; Fig. 1 & S1, Table S2, campaign number: 37 (green)). The M10 circumnavigation data are split spatiotemporally into 3 datasets, each broadly covering different ocean basins (Fig. 1 & S1, Table S2, campaign numbers: 30 (M10a, black), 31 (M10b, dark red), 32 (M10c, cyan)).

2.2 Ancillary *in-situ* & coincident satellite measurements

Ancillary *in-situ* and remotely sensed data are used to explore the potential mechanisms driving DMS variability. *In-situ* sea surface salinity (hereafter salinity) and temperature (SST) from each DMS dataset are used to derive sea surface density (hereafter density) (see Fernandes, 2014).

Satellite monthly mean chlorophyll-a (Chl) and 5-day sea surface height anomaly (SSHA) data are matched to the average date of each DMS sampling cruise. Satellite data pixels are extracted along the coordinates of the DMS cruise track using the NASA SeaDAS software (version 7.5.3). NASA MEaSUREs L4 0.17° 5-day SSHA are used to explore the role of eddies in driving DMS variability (Zlotnicki et al., 2019). NASA MODIS-Aqua L3 4 km monthly Chl is used as a proxy for plankton biomass and biological productivity (NASA Goddard Space Flight Center, 2018).

2.3 Data processing

Underway data are screened to only include data acquired when ship speed was >1 m s^{-1}, to avoid measurements made when ships were sampling on station. Ship speed is calculated from distance and time between measurements. Each DMS dataset and all its ancillary data is divided into transects. Transects are defined as continuous data sections with a minimum sampling frequency of 1 hour. Most observations (83%) captured by the temporal filter are <2.2 km apart. The minimum transect length is calculated in two stages: 1) the linear distance between the start and end of a continuous data section must be >100 km to avoid campaigns that targeted a specific area multiple times (e.g., a productive bloom or mesoscale eddy); 2) each dataset is divided into equal length transects, with an along track distance of at least 100 km. The initial data processing yields 1039 continuous transects from 37 DMS campaigns, with each transect 100–199 km in cumulative length (Fig. 1).

2.4 Variability lengthscale (VLS) analysis

Previous DMS VLS studies have not applied a standardised or consistent approach (Asher et al., 2011; Nemcek et al., 2008; Royer et al., 2015; Tortell, 2005b; Tortell et al., 2011; Tortell & Long, 2009). The analysis presented here adopts the method used to study the VLS of seawater CO_2 (Hales & Takahashi, 2004), which was later applied to DMS by Tortell et al. (2011) and Nemcek et al. (2008).

The highest observational DMS sampling resolution in the datasets is typically between 0.2 and 2.2 km. Each data transect is subsampled repeatedly starting from the first data point, at increasingly coarse spacings ranging from 2.2 km to half the length of the transect (the lowest possible resolution), increasing in 0.2 km increments. At each subsampling resolution, the first and last subsampled points of the data transect define the subsampling window. Subsampled data across the subsampling window are linearly interpolated to the resolution of the original data. Where the subsampling window matches the length of the data transect, the interpolation error associated with the subsampling resolution is calculated as the root mean squared error (RMSE) between the original and the interpolated values. Where the subsampling window is not equal to the length of the transect, the window is shifted along the transect, incrementing by one data point, and the transect is re-subsampled. Re-subsampled data are linearly interpolated across the shifted window, and the RMSE is re-calculated. The subsampling window is repeatedly shifted along the data transect and interpolation RMSE re-calculated until the subsampling ends on last data point of the transect. The error associated with the subsampling resolution is taken as the average of all the RMSE values produced by sliding the window across the data transect at that resolution. RMSE is calculated following Eq. (1):

$$RMSE = \sqrt{\overline{(Obs - Interp)^2}} \tag{1}$$

RMSE typically increases in proportion to the coarseness of the subsampling until a maximum error plateau, or asymptote, is reached. The maximum error plateau corresponds to the total variance of the dataset (Belviso et al., 2004; Tortell et al., 2011).

The trend in RMSE as a function of subsampling resolution is well described by a non-linear first-order inverse exponential rise function following Eq. (2):

$$E_x = E_\infty \left(1 - e^{\left(-\frac{x}{\text{VLS}}\right)}\right) \qquad (2)$$

where E_x is the interpolation error at subsampling resolution x, E_∞ is the asymptotic maximum interpolation error at an infinite subsampling resolution, and VLS is the characteristic lengthscale of variability. VLS is determined by the sub-sampling resolution (interpolation distance) where a tangent of the initial slope intersects with the maximum error (E_∞, Fig. 2). VLS also corresponds to the intersect on the curve (E_x) that is 63% of E_∞, i.e., Eq. (3):

$$\frac{E_x}{E_\infty} = 1 - e^{\left(-\frac{x}{\text{VLS}}\right)} \approx 0.63 \qquad (3)$$

Previous work suggested that a sudden change (or 'breakpoint') in the RMSE slope can be used to characterise the DMS VLS (Asher et al., 2011; Royer et al., 2015). However, this approach is unreliable, because the data assessed in this study shows that the breakpoint does not always occur, and its identification is subjective (see Table S1, Supplementary Material).

An inverse exponential rise function (Eq. 2&3) is used here to objectively derive VLS. The objective VLS method is applied to all 1039 transects and six variables: DMS, SST, salinity, density, Chl, SSHA.

2.4.1 Quality assurance and VLS statistics

Two filters are used to identify viable data transects. VLS is rejected if the distance is greater than the maximum subsampling / interpolation distance (equal to half the transect length), which only occurred in very noisy datasets. The second filter is the quality of fit to the data using the residual standard error (RSE) (Fig. 2b), which is defined as $\text{RSE} = \sqrt{(ss_{res}/n)}$ where n is the number of data points in the transect and ss_{res} is the sum of the squares of the residuals, i.e., $ss_{res} = \sum(residuals\ from\ fitted\ curve)^2$.

The RSE is normalised using the maximum RSE of the curve (i.e., (RSE/RSE at the asymptote) $\times$ 100) and if the normalised RSE exceeds 10%, the curve is deemed to inadequately describe the data and the transect is rejected. The two quality control filters reduce the initial 1039 transects to 763 'viable' transects.

The distributions of VLS from the 763 transects are skewed for all parameters (Fig. 3 & S2). The geometric mean and geometric standard deviation (GSD) are computed to assess central tendency and spread while accounting for skew in the data. Note that the geometric mean is regularly referred to as the 'average' within this manuscript to aid readability. All significance testing uses the non-parametric Mann-Whitney U Test. Transects are grouped and averaged by sampling campaign to assess underlying spatial and temporal (regional and seasonal) patterns of variability. Average VLS distances are calculated for each

sampling campaign and for all variables (VLS_{DMS}, VLS_{SST}, $VLS_{salinity}$, $VLS_{density}$, VLS_{Chl}, VLS_{SSHA}). A minimum threshold of four transects was necessary before calculating a campaign average VLS. Exclusion of campaigns with <4 transects reduced the total number of campaigns from 37 to 35.

190   Correlation and multiple linear regression (MLR) are used to explore the global controls on VLS_{DMS} (see Sect. 3.3.1 and 3.3.2; Table 1). The campaign average VLS used in each correlation and regression analysis only includes transects where coincident VLS can be calculated from the DMS and non-DMS variables. MLR models with two input variables contain 20-26 datasets, and MLR models with three input variables contain 11-15 datasets (see Table 1). The relative importance of the input variables in each MLR model are calculated based on the incremental R^2 used to determine interactional dominance (defined as the

195   incremental R^2 contribution of each predictor to the complete model; Azen & Budescu, 2003).

3 Results

3.1 Global VLS statistics

The global average DMS concentration and geometric standard deviation (GSD) for the viable transects covered in this study are 2.23 nM (average) and 2.29 (GSD), which is similar to the global average and GSD from the GSSDD (2.66 nM (average),

200   2.88 (GSD); date of last access 15 April 2022). The similarity between the two datasets suggests that the data used in this study is representative of global observations. The global average and GSD of VLS_{DMS} from all 763 transects are 12.57 km and 2.33, respectively (Fig. 3). Global average VLS_{DMS} is the smallest of the six variables tested, with VLS_{SSHA} the most similar (15.76 km, 1.77 GSD) (Fig. 3). Global average VLS_{Chl} is slightly larger (20.89 km, 1.67 GSD) and similar to global average $VLS_{density}$ (20.21 km, 1.76 GSD), and its components VLS_{SST} (21.23 km, 1.73 GSD) and $VLS_{salinity}$ (19.52 km, 1.84 GSD) (Fig. 3 & S1).

205   Global average VLS_{DMS} and VLS_{SSHA} are significantly different ($p < 0.01$) from each other and the global average VLS of all other parameters. Global average VLS_{Chl}, $VLS_{density}$, VLS_{SST}, and $VLS_{salinity}$ are not significantly different from one another.

All six variables have an average spatial variability that is tens of kilometres in all regions. Global average VLS_{SSHA} is similar (within 4 km) to global average VLS_{DMS}. Global average VLS for all other parameters are within 9 km of global average

210   VLS_{DMS}. Campaign average VLS_{DMS} ranges from 2 to 30 km, which is the same order of magnitude as the range of 7–50 km reported by other DMS variability studies (Asher et al., 2011; Nemcek et al., 2008; Royer et al., 2015; Tortell, 2005b; Tortell et al., 2011). Note that a detailed comparison between studies should be treated with caution because each have used different methods to identify the VLS.

3.2 Regional patterns of DMS variability

215   VLS_{DMS} is generally small in the subtropical gyres, specifically the equatorial and subtropical South Pacific and South Atlantic (Fig. 4; see Table S2 for each sampling campaign average VLS_{DMS}, e.g., campaign numbers: 30, M10a, black; 31, M10b, dark

red; and 32, M10c, cyan). The average VLS_{DMS} from all transects in the three M10 low–mid latitude circumnavigation campaign datasets (mean = 6.34 km, GSD = 2.59) is consistently smaller than the global value (mean = 12.57 km, GSD = 2.33) (Fig. 4). The relative homogeneity of small VLS_{DMS} in these oligotrophic domains is not replicated in the VLS of any other variables (Fig. S3). The Southern Hemisphere subtropical gyres are permanently stratified biomes, bounded to the south by a band of seasonally stratified biomes (Fay & McKinley, 2014). At the boundary transitions from permanently to seasonally stratified conditions there are some notable exceptions to the low VLS_{DMS}, e.g., the Benguela upwelling (southeast Atlantic) and South Australia upwelling (Fig. 4).

In contrast, the average (mean = 22.06 km, GSD = 1.60) of VLS_{DMS} in the Peruvian upwelling (East equatorial Pacific) is consistently larger than the global average (mean = 12.57 km, GSD = 2.33) (Fig. 4). Larger VLS_{DMS} is also found along parts of the Pacific and Atlantic coastlines of North America, with smaller VLS_{DMS} further offshore (Fig. 4, inset). VLS_{DMS} in the Arctic, northeast Pacific, northwest Atlantic, and southeast Indian open ocean regions are highly variable. The Southern Ocean has VLS_{DMS} generally below the global average and features some localised pockets with larger VLS (Fig. 4). DMS concentration variability in mid–high latitude regions is seasonal (Hulswar et al., 2022) and VLS_{DMS} could be influenced by the season / time of year.

3.3 Drivers of DMS variability

3.3.1 Transect and campaign average VLS regressions

Simple linear regressions are used to explore the relationship between VLS_{DMS} and VLS for SST, salinity, density, Chl and SSHA. The possibility of a relationship with latitude (as discussed in Royer et al. (2015)) is also investigated. Transect and campaign average VLS_{DMS} do not vary with latitude (R^2 = 0.02, n = 35, *p > 0.05;* Table 1). No significant relationships are observed between transect VLS_{DMS} and VLS for SST, SSS, density, Chl and SSHA. Averaging transect VLS data into campaign averages reduces the noise and enables statistically significant relationships to be identified. Campaign average $VLS_{density}$ explains 37% of the variations in VLS_{DMS} (Table 1; Fig. 5a). VLS_{SSHA} (used as an indicator of the dynamic eddy field in the open ocean) and VLS_{Chl} each explain approximately half of the campaign average VLS_{DMS} (46% and 47%, respectively; Table 1; Fig. 5b&c).

3.3.2 Multiple linear regression of VLS_{DMS}

Multiple linear regression (MLR) is used on the campaign average VLS for SST, salinity, density, Chl and SSHA to explore VLS_{DMS} variance (Table 1; see Table S4, Supplementary Material for regression coefficients). Eleven MLR combinations were tested, and all results are significant (*p* <0.01) except for the combination of VLS_{Chl}, VLS_{SSHA} and VLS_{SST} (Model 17, Table 1). Note that the number of available datasets is reduced in the MLR models that have more input variables, which results in the contribution of fewer data (campaigns) to the result. The number of input data is substantially increased if campaign

averages are calculated without filtering the data prior to correlation so they only contain data where the two or more correlated variables are co-located. Relaxing the criteria such that the transects need not be coincident increases the number of campaigns

250 that can be included in each MLR model. The 'relaxed criterion' approach is less robust but gives similar results to those presented here (see Table S3, Supplementary Material).

Individual VLS_{Chl} and/or VLS_{SSHA} regressions with VLS_{DMS} are outperformed (i.e., $R^2 > 0.47$) by four MLR combinations (Models 7-10, Table 1). The combination of $VLS_{density}$ and VLS_{Chl} (Model 9, Table 1) substantially improves the regression with VLS_{DMS} (adjusted R^2 increases to 0.63). MLR Model 9 has the most campaigns (n = 26) of any model, and the third

255 highest number of available data transects (n = 224). VLS_{Chl} (54%) and $VLS_{density}$ (46%) make approximately equal contributions to the changes in VLS_{DMS} described by Model 9.

The largest amount of VLS_{DMS} variability explained by the MLR models uses the combination of VLS_{SSHA}, VLS_{Chl} and $VLS_{density}$, improving the adjusted R^2 to 0.77 (Model 7, Table 1; Fig. 5d). VLS_{SSHA} is the dominant parameter in Model 7 (52%

260 of the explained variance), with VLS_{Chl} and $VLS_{density}$ accounting for 34% and 14%, respectively. Combining VLS_{Chl} and VLS_{SSHA} (MLR Model 11) reduces the available input data (n = 20) and does not increase the explained variance in VLS_{DMS} compared to using only one or other of the input parameters. VLS_{SSHA} and VLS_{Chl} dominate the explained variance in MLR models when paired with one other variable (Models 12–16, Table 1).

4 Discussion

265 ### 4.1 Global statistics

This is the first study of sub-mesoscale seawater DMS variability from a global perspective. Spatial variability lengthscale analysis is applied to every ocean basin, and at different times of year, using a consistent methodology. Characteristic spatial variability in all six variables (DMS, SST, salinity, density, Chl, SSHA) occurs at the low mesoscale (in the tens of kilometres) in all regions. Campaign average VLS_{DMS} ranges from 2-30 km (Table S2, Supplementary Material), in general agreement

270 with previous work (Asher et al., 2011; Nemcek et al., 2008; Royer et al., 2015; Tortell, 2005b; Tortell et al., 2011; Tortell & Long, 2009). There is no correlation between campaign average DMS concentration and VLS_{DMS} ($R^2 = 0.01$, *p > 0.05*), which suggests that understanding the variability may be a helpful and independent approach to understanding the processes that control surface ocean DMS.

4.2 Regional patterns of DMS variability

275 VLS_{DMS} is generally above average at the edge of ocean basins e.g., parts of northwest Atlantic, northeast Pacific, the California coast (Fig. 4, inset). It may be possible that the longer lengthscales of coastal DMS spatial variability are driven by large phytoplankton blooms, which previous local/regional studies suggest can dominate coastal domains (Asher et al., 2011; Nemcek et al., 2008). This work does not investigate the detail of drivers of DMS variability in individual regions or domains.

Open ocean domains such as the sub-tropical gyres in the Southern Hemisphere have generally small VLS_{DMS}, a feature not evident in the VLS of the other parameters (Fig. 4 & S2). Short lengthscales of DMS variability in stable stratified biomes offers the opportunity for future work to re-examine these regions for as yet unidentified drivers of variability. Most low latitude DMS data used in this study originate from a single sampling campaign (e.g., Malaspina Expedition 2010; Royer et al., 2015). To test if small VLS_{DMS} is a persistent feature in under-sampled sub-tropical open oceans, more high-resolution observations are needed.

Factors driving temporal DMS variability are not explored in this study. However, complex VLS_{DMS} fluctuations at high latitudes (e.g., northwest Atlantic, northeast Pacific, Southern Ocean; Fig. 4) may be capturing variations in both space and time. VLS_{DMS} in high latitude dynamic regions could be related to the seasonality of biological productivity and eddy activity (see Asher et al., 2011; Behrenfeld et al., 2019; Bell et al., 2021; Fox et al., 2020; Gaube et al., 2019; Herr et al., 2019; Lana et al., 2011; McGillicuddy, 2016). Additionally, it is plausible that VLS_{DMS} in the polar regions may be sensitive to the seasonal impact of sea ice on biogeochemical processes (see Galí et al., 2021; Lannuzel et al., 2020; Stefels et al., 2018). There are not enough repeat measurements made in high latitude (high seasonal variability) regions to establish the impact of seasonality on VLS_{DMS}. In this study, the only region sampled during different seasons is the northwest Atlantic (4 Atlantic NAAMES campaigns; Bell et al., 2021) and there is not yet compelling evidence of a temporal difference between the VLS_{DMS} of these cruises/seasons. VLS_{DMS} of the NAAMES 1 transects (November; average = 11.93 km, GSD = 1.76) are significantly different (p <0.01) from the transect VLS_{DMS} of NAAMES 3 ($U = 99$, p <0.01; September; average = 20.89 km, GSD = 1.69) and NAAMES 4 ($U = 89$, p <0.01; March/April; average = 21.94 km, GSD = 1.57), but not from NAAMES 2 ($U = 108$, $p = 0.014$; May/June; average = 18.4 km, GSD = 1.56). VLS_{DMS} of the NAAMES 2, 3 & 4 transects are not significantly different from each other (all p >0.2).

4.3 Drivers of DMS variability

The variance in campaign average VLS_{DMS} data explained by physical processes (represented by VLS_{SSHA}) is as important as biogeochemical processes (represented by VLS_{Chl}), with each parameter able to explain just under half of the VLS_{DMS} (Models 1&2, Table 1; Fig. 5). This conclusion contrasts with the findings of Royer et al. (2015) who find in the low–mid latitudes the majority of VLS_{DMS} (65%) are more similar to the VLS of biological variables that represent biomass and physiology (Chl and fluorescence) than to the VLS of physical variables. These contrasting conclusions potentially reflect the fact that length scales of physical oceanographic variability increase towards the equator, due to the effects of the Earth's rotation. The Coriolis parameter and therefore Rossby radius are intrinsically latitudinal dependent (Jacobs et al., 2001). The longer transects used by Royer et al. (2015) at low–mid latitudes enable them to capture scales of variability that may be associated with large physical features. This point is discussed further in in Sect. 4.5.

A larger proportion of campaign average VLS_{DMS} variability (77%) can be explained using VLS_{Chl}, VLS_{SSHA} and $VLS_{density}$ (Model 7, Table 1) compared to just VLS_{SSHA} or VLS_{Chl}. The data included in the $VLS_{SSHA-Chl-Density}$ MLR (Model 7, Table 1) is a subset but includes at least one campaign from each major ocean basin (Fig. S4, Supplementary Material) and is thus a significant relationship with global applicability. VLS_{SSHA} explains the majority of VLS_{DMS} in the $VLS_{SSHA-Chl-Density}$ MLR (52%) (Model 7, Table 1) and improves the prediction of changes in VLS_{DMS} compared to using just VLS_{Chl} and $VLS_{density}$ (Model 9, Table 1). The $VLS_{SSHA-Chl-Density}$ MLR (Model 7, Table 1) includes measurements from the NAAMES4 (2018) cruise, which targeted a substantive eddy and observed a persistent high Chl feature coincident with elevated DMS levels (Bell et al., 2021). The water mass within an eddy tends to be retained by the circulation, such that plankton within the eddy are accumulated under relatively stable physics (upwelling or downwelling) and consistent biogeochemical conditions (Bell et al., 2021). Eddies may thus drive conditions where DMS variability is closely associated with biological activity and a clear co-variation in VLS is observed, even if the relationship between DMS and Chl concentration is less obvious (della Penna & Gaube, 2019). The relationship between eddy structure, biogeochemistry and DMS may explain the link between changes in VLS_{DMS}, VLS_{SSHA}, and VLS_{Chl}. The importance of VLS_{SSHA} for predicting VLS_{DMS} is consistent with results recently reported by McNabb & Tortell (2022), who apply two independent machine learning techniques to analyse DMS in the northeast Pacific. McNabb & Tortell (2022) demonstrate the power of mesoscale eddies for predicting DMS variability (Spearman correlation coefficients = 0.35 and 0.42, depending on the machine learning method employed), using the same SSHA product used in this study (using only summertime measurements, 1997 – 2017). The $VLS_{SSHA-Chl-Density}$ MLR model coefficients (Model 7, Table S4, Supplementary Material) are used to predict VLS_{DMS} for the target input data subset (Fig. 5d). The residuals of predicted VLS_{DMS} are not systematically biased within the full range of the data (5 – 25 km).

4.4 Implications for global DMS parameterisation

Low resolution measurements have previously been used to predict mean spatiotemporal patterns of DMS, both regionally and globally. Several studies have parameterised DMS as a function of surface mixed layer depth (MLD), light, and Chl (Anderson et al., 2001; Aranami & Tsunogai, 2004; Aumont et al., 2002; Belviso, Moulin, et al., 2004; Galí et al., 2018; Simó & Dachs, 2002; Vallina & Simó, 2007). For example, Simó & Dachs (2002) use climatological MLD and remotely sensed Chl to estimate average DMS concentrations, while Vallina & Simó (2007) use climatological MLD, surface irradiance and light attenuation to estimate surface DMS from the 'solar radiation dose'. Galí et al. (2018) employ an algorithm driven by climatological Argo MLD and satellite derived Chl, SST, and photosynthetically active radiation (PAR). Only the latter algorithm was additionally validated at finer resolution using non-climatological data to enable regional timeseries studies (Galí et al., 2019). SSHA reflects surface mixing and changes to the MLD (Gaube et al., 2019). This study supports the choice of key variables used in existing empirical parameterisations by demonstrating that, even on small scales, physical mixing (SSHA, density) and biological activity (Chl) explain a large portion of surface seawater DMS spatial variability in the global ocean.

DMS parameterisations with global coverage that rely on remote and autonomous observations predict spatially and seasonally averaged surface seawater DMS reasonably well (e.g., Galí et al., 2018; Simó & Dachs, 2002; Vallina & Simó, 2007). However, some studies have questioned whether such parameterisations are overly reliant on spatial/temporal averaging, often to 1°/monthly resolution (e.g., Derevianko et al., 2009). The spatiotemporal averaging used to develop global parameterisations may lead to an over-confidence in current predictive capabilities because key parameters are not included. Statistically significant MLR relationships in this study are obtained once the transect data are averaged by campaign, and the average VLS for all six variables in our study is tens of kilometres. Using VLS analysis to assess the covariation of parameters at the sub-mesoscale provides insights that can help to improve global parameterisations. Our results indicate that patterns of mesoscale and sub-mesoscale DMS variability, particularly those associated with SSHA, will be obscured at the 1° resolution of most global parameterisations, highlighting the importance of modelling work at finer resolutions (e.g., Galí et al., 2019; McNabb & Tortell, 2022, 2023). Regional studies have tested empirical predictive relationships for DMS with varying degrees of success (Asher et al., 2011; Bell et al., 2006, 2021; Royer et al., 2015).

4.5 Study limitations and unidentified drivers of DMS variability

This work provides as comprehensive assessment of DMS variability across the global ocean as existing data allow, yet many regions have not yet been sampled at high enough resolution to permit an assessment of VLS_{DMS}. For example, only seven of the 37 campaigns in this study have made high resolution DMS measurements in low latitude waters (30ºN–30ºS). There is a seasonal sampling bias within the DMS database, and the northwest Atlantic is the only region to have been assessed for VLS throughout the seasonal cycle (Bell et al., 2021). More data are needed.

Satellite-derived VLS_{Chl} and VLS_{SSHA} have been used to predict VLS_{DMS} (e.g., Model 7, Table 1), but this relies on the assumption that the satellite-retrieved data are representative of phytoplankton productivity and eddy activity throughout the research cruise/campaign. Satellite retrievals for Chl with higher than monthly temporal resolution or, in the case of SSHA, higher than 0.17º spatial resolution, may improve the ability to explain variance in VLS_{DMS}.

Transect lengths between 100 and 199 km are used to ensure comparability between datasets/regions because VLS results from previous studies appear to be sensitive to the length of data transect (see Fig. S5, Supplementary Material). However, by limiting the transect length, it is difficult to identify large eddies using VLS_{SSHA}. Eddy length scales are typically larger at low latitudes due to the dependence of the Coriolis parameter on latitude (Chelton et al., 1998). The maximum VLS in this study is between 50 and 99.5 km (half the transect length), which is long enough to capture the eddy variability at latitudes where the eddy length scale is related to the Rossby radius of deformation, i.e., poleward of 30º where the deformation radius is < 30 km (Eden, 2007). Equatorward of 30º eddy length scales are not well predicted by the Rossby radius of deformation and can exceed 50 km (Eden, 2007; Klocker et al., 2016; Rhines, 1975; Scott & Wang, 2005; Tulloch et al., 2011). The VLS_{SSHA} analysis approach used in this study is designed to identify the dominant scale of variability in physical features up to 50–99.5

km, therefore it may not capture the full extent of variability associated with large eddies at low latitudes. Large eddies will however still be captured in the VLS_{SSHA} analysis where a transect segments an eddy without passing through its centre. We also note that although SSHA is used to represent eddy features, at the equator stratification and strong westward currents tend to dominate SSHA variability rather than rotation and eddy transport (Williams & Follows, 2011).

VLS_{DMS} in the subtropical gyres is typically small (<10 km; Fig. 4), which is qualitatively consistent with the short (days) response time of DMS to perturbations in the dynamic equilibrium of DMS production and consumption in these waters (Galí & Simó, 2015). VLS_{DMS} in subtropical waters does not correspond well with the VLS of any of the other parameters (Fig. S3, Supplementary Material). Cycling of reduced sulfur compounds in sub-tropical waters is well-documented to be part of a different biogeochemical regime compared to productive, higher latitude waters (e.g., Galí & Simó, 2015; Toole & Siegel, 2004). In stable oligotrophic regions where there is less variability in physical mixing and phytoplankton productivity, VLS_{DMS} could thus be dominated by alternative parameters that drive variability in the biological cycling of DMS such as zooplankton grazing (Simó et al., 2018) and microbial organosulfur metabolism (Alcolombri et al., 2015; Cui et al., 2015; Nowinski et al., 2019).

The so-called 'summer paradox' describes the seasonal misalignment between maximum concentrations of phytoplankton biomass and DMS in low latitude waters and has been challenging to model (e.g., Galí & Simó, 2015; Polimene et al., 2012; Toole et al., 2008; Vallina et al., 2008). In these areas, characterized by low seasonal amplitude in phytoplankton biomass, changes in phytoplankton species succession and physiological stress control DMS production yields and rates, and ultimately DMS seasonality. By contrast, aggregated loss processes exhibit low seasonal variability and are insufficient to explain large-scale DMS seasonality in 'summer paradox' areas (Galí & Simó, 2015). Previous studies observed important short-term variations in the balance between DMS sources and sinks in oligotrophic waters, concomitant with meteorological forcing (Royer et al., 2016). Hence, it is plausible to hypothesize that subtle changes in this balance can explain some of the variance in VLS_{DMS}. Light exposure in surface waters influences plankton physiological production and stress, photochemical reactions, and bacterial activity, and thus has a significant impact on the cycling of reduced sulfur in oligotrophic regions (see Toole & Siegel, 2004; Vallina et al., 2008). These factors have not been included in the present study.

5 Conclusions

This study presents a comprehensive and objective analysis of DMS variability based on a large global dataset of high frequency observations at the local/regional scale. The work shows that the variability lengthscale for DMS is typically small (< 30 km) and that a substantial proportion of the campaign average variance can be explained by the VLS of key biological (Chl) and physical (density, SSHA) observations (Model 7, Table 1). The results improve confidence in the validity of the biological and physical parameters used to currently parameterise seawater DMS at large scales and used in many global

climate models (e.g., Bock et al., 2021; Galí et al., 2018; Mulcahy et al., 2020; Simó & Dachs, 2002). However, there is substantial variability in VLS_{DMS} when assessing individual transects, which suggests that unaccounted-for variables are also important (e.g., light, wind speed, microbial diversity and activity). Making high frequency measurement of these parameters at the same time as high frequency DMS measurements may help elucidate their role in DMS cycling.

Data availability

DMS and ancillary *in-situ* data (SST and salinity) are sourced from the global surface seawater DMS database (GSSDD; https://saga.pmel.noaa.gov/dms/; last access: 15 April 2022), and supplied by authors RS, MG, and ASM (Malaspina Expedition in 2010-2011, M10), TB (North Atlantic Aerosol and Marine Ecosystem Study in 2015–2018, NAAMES; https://doi.org/10.5067/SeaBASS/NAAMES/DATA001), and GM (Southern oCean SeAsonaL Experiment in 2019, SCALE). Requests for access to M10 and SCALE DMS data can be sent to the corresponding authors (GM and TB). Satellite data are available in online NASA repositories for chlorophyll-*a* (https://doi.org/10.5067/AQUA/MODIS/L3M/CHL/2018) and sea surface height anomalies (https://doi.org/10.5067/SLREF-CDRV2).

Supplement

The supplement related to this article is available online at: … [insert DOI]

Author contributions

GM, PH, TB and JPM devised the study. GM conducted the analysis and interpretation, and wrote the manuscript, with input from PH and TB. JPM, MG, and RS provided insight and helped improve the analysis and interpretation. All co-authors contributed to the manuscript.

Competing interests

The authors declare that they have no conflict of interest.

Acknowledgements

This work was supported by the UK Natural Environmental Research Council (through a PhD studentship for GM: NE/R007586/1). The contribution of TB was via the NAAMES (a NASA Earth Venture Suborbital program, NNX#15AF31G) and CARES (NERC: NE/W009277/1) projects. JPM was supported by the Met Office Hadley Centre Climate Programme funded by BEIS and also received funding from the European Union's Horizon 2020 research and innovation programme

under grant agreement n°101003536. This research was supported by the Spanish national funding plan for science through project BIOGAPS (CTM2016-81008-R) to RS, through project DMS-Cons (202230I123) to MG, and through the 'Severo Ochoa Centre of Excellence' grant (CEX2019-000928-S) to the ICM-CSIC. RS is a holder of a European Research Council Advanced Grant (ERC-2018-ADG-834162) under the EU's Horizon H2020 research and innovation programme. The Indian Institute of Tropical Meteorology is funded by the Ministry of Earth Sciences, Government of India.

We thank the contributors of high frequency DMS data (Archer, Herr, Jarnikova, Johnson, Marandino, Royer, Saltzman, Tortell, and Zhang) for making their DMS data available (see Table S2, Supplementary Material for full details) via the Global Surface Seawater DMS Database. GM and TB thank those involved in the 2019 SCALE (Southern oCean SeAsonaL Experiment) spring–summer campaign, including Chief Scientists Dr Thomas Ryan-Keogh and Professor Marcello Vichi, Captain Knowledge Bengu, and the crew of the SA Agulhas II. Special thanks go to Chief Scientist Dr Sandy Thomalla for facilitating GM and TB's involvement in the SCALE project, and to Tebatso Martin Moloto for assisting GM in the onboard measurement of DMS.

References

Alcolombri, U., Ben-Dor, S., Feldmesser, E., Levin, Y., Tawfik, D. S., & Vardi, A. (2015). Identification of the algal dimethyl sulfide-releasing enzyme: A missing link in the marine sulfur cycle. *Science*, *348*(6242), 1466–1469. https://doi.org/10.1126/SCIENCE.AAB1586

Anderson, T. R., Spall, S. A., Yool, A., Cipollini, P., Challenor, P. G., & Fasham, M. J. R. (2001). Global fields of sea surface dimethylsulfide predicted from chlorophyll, nutrients and light. *Journal of Marine Systems*, *30*(1–2), 1–20. https://doi.org/10.1016/S0924-7963(01)00028-8

Aranami, K., & Tsunogai, S. (2004). Seasonal and regional comparison of oceanic and atmospheric dimethylsulfide in the northern North Pacific: Dilution effects on its concentration during winter. *Journal of Geophysical Research D: Atmospheres*, *109*(12), 1–15. https://doi.org/10.1029/2003JD004288

Asher, E. C., Merzouk, A., & Tortell, P. D. (2011). Fine-scale spatial and temporal variability of surface water dimethylsufide (DMS) concentrations and sea-air fluxes in the NE Subarctic Pacific. *Marine Chemistry*, *126*(1–4), 63–75. https://doi.org/10.1016/j.marchem.2011.03.009

Aumont, O., Belviso, S., & MONFRAY, P. (2002). Dimethylsulfoniopropionate (DMSP) and dimethylsulfide (DMS) sea surface distributions simulated from a global three-dimensional ocean carbon cycle model. *Journal of Geophysical Research*, *107*(C4). https://doi.org/10.1029/1999jc000111

Azen, R., & Budescu, D. v. (2003). The Dominance Analysis Approach for Comparing Predictors in Multiple Regression. *Psychological Methods*, *8*(2), 129–148. https://doi.org/10.1037/1082-989X.8.2.129

465   Bates, T. S., Lamb, B. K., Guenther, A., Dignon, J., & Stoiber, R. E. (1992). Sulfur emissions to the atmosphere from natural sources. *Journal of Atmospheric Chemistry*, *14*(1–4), 315–337. https://doi.org/10.1007/BF00115242

Behrenfeld, M. J., Moore, R. H., Hostetler, C. A., Graff, J., Gaube, P., Russell, L. M., Chen, G., Doney, S. C., Giovannoni, S., Liu, H., Proctor, C., Bolaños, L. M., Baetge, N., Davie-Martin, C., Westberry, T. K., Bates, T. S., Bell, T. G., Bidle, K. D., Boss, E. S., … Ziemba, L. (2019). The North Atlantic Aerosol and Marine Ecosystem Study (NAAMES): Science

470   motive and mission overview. *Frontiers in Marine Science*, *6*(MAR), 122. https://doi.org/10.3389/FMARS.2019.00122/BIBTEX

Bell, T. G., Malin, G., Lee, G. A., Stefels, J., Archer, S., Steinke, M., & Matrai, P. (2012). Global oceanic DMS data inter-comparability. *Biogeochemistry*, *110*(1–3), 147–161. https://doi.org/10.1007/s10533-011-9662-3

Bell, T. G., Malin, G., McKee, C. M., & Liss, P. S. (2006). A comparison of dimethylsulphide (DMS) data from the Atlantic

475   Meridional Transect (AMT) programme with proposed algorithms for global surface DMS concentrations. *Deep-Sea Research Part II: Topical Studies in Oceanography*, *53*(14–16), 1720–1735. https://doi.org/10.1016/j.dsr2.2006.05.013

Bell, T. G., Porter, J. G., Wang, W. L., Lawler, M. J., Boss, E., Behrenfeld, M. J., & Saltzman, E. S. (2021). Predictability of Seawater DMS During the North Atlantic Aerosol and Marine Ecosystem Study (NAAMES). *Frontiers in Marine Science*, *7*, 1200. https://doi.org/10.3389/FMARS.2020.596763/BIBTEX

480   Belviso, S., Bopp, L., Moulin, C., Orr, J. C., Anderson, T. R., Aumont, O., Chu, S., Elliott, S., Maltrud, M. E., & Simó, R. (2004). Comparison of global climatological maps of sea surface dimethyl sulfide. *Global Biogeochemical Cycles*, *18*(3). https://doi.org/10.1029/2003GB002193

Belviso, S., Moulin, C., Bopp, L., & Stefels, J. (2004). Assessment of a global climatology of oceanic dimethylsulfide (DMS) concentrations based on SeaWiFS imagery (1998-2001). *Canadian Journal of Fisheries and Aquatic Sciences*, *61*(5),

485   804–816. https://doi.org/10.1139/f04-001

Bock, J., Michou, M., Nabat, P., Abe, M., Mulcahy, J. P., Olivié, D. J. L., Schwinger, J., Suntharalingam, P., Tjiputra, J., van Hulten, M., Watanabe, M., Yool, A., & Séférian, R. (2021). Evaluation of ocean dimethylsulfide concentration and emission in CMIP6 models. *Biogeosciences*, *18*(12), 3823–3860. https://doi.org/10.5194/BG-18-3823-2021

Boucher, O., Moulin, C., Belviso, S., Aumont, O., Bopp, L., Cosme, E., von Kuhlmann, R., Lawrence, M. G., Pham, M.,

490   Reddy, M. S., Sciare, J., & Venkataraman, C. (2003). DMS atmospheric concentrations and sulphate aerosol indirect radiative forcing: a sensitivity study to the DMS source representation and oxidation. *Atmospheric Chemistry and Physics*, *3*(1), 49–65. https://doi.org/10.5194/acp-3-49-2003

Carslaw, K. S., Lee, L. A., Reddington, C. L., Pringle, K. J., Rap, A., Forster, P. M., Mann, G. W., Spracklen, D. v., Woodhouse, M. T., Regayre, L. A., & Pierce, J. R. (2013). Large contribution of natural aerosols to uncertainty in indirect

495   forcing. *Nature*, *503*(7474), 67–71. https://doi.org/10.1038/nature12674

Charlson, R. J., Lovelock, J. E., Andreae, M. O., & Warren, S. G. (1987). Oceanic phytoplankton, atmospheric sulphur, cloud albedo and climate. *Nature*, *326*(6114), 655–661. https://doi.org/10.1038/326655a0

Chelton, D. B., deSzoeke, R. A., Schlax, M. G., Naggar, K. el, & Siwertz, N. (1998). Geographical Variability of the First Baroclinic Rossby Radius of Deformation. *Journal of Physical Oceanography*, *28*(3), 433–460. https://doi.org/10.1175/1520-0485(1998)028

Chu, S., Elliott, S., & Maltrud, M. E. (2003). Global eddy permitting simulations of surface ocean nitrogen, iron, sulfur cycling. *Chemosphere*, *50*(2), 223–235. https://doi.org/https://doi.org/10.1016/S0045-6535(02)00162-5

Cui, Y., Suzuki, S., Omori, Y., Wong, S. K., Ijichi, M., Kaneko, R., Kameyama, S., Tanimoto, H., & Hamasaki, K. (2015). Abundance and distribution of dimethylsulfoniopropionate degradation genes and the corresponding bacterial community structure at dimethyl sulfide hot spots in the tropical and subtropical Pacific Ocean. *Applied and Environmental Microbiology*, *81*(12), 4184–4194. https://doi.org/10.1128/AEM.03873-14/FORMAT/EPUB

della Penna, A., & Gaube, P. (2019). Overview of (sub)mesoscale ocean dynamics for the NAAMES field program. *Frontiers in Marine Science*, *6*(JUL), 384. https://doi.org/10.3389/FMARS.2019.00384/BIBTEX

Derevianko, G. J., Deutsch, C., & Hall, A. (2009). On the relationship between ocean DMS and solar radiation. *Geophysical Research Letters*, *36*(17). https://doi.org/10.1029/2009GL039412

Eden, C. (2007). Eddy length scales in the North Atlantic Ocean. *Journal of Geophysical Research: Oceans*, *112*(C6), 6004. https://doi.org/10.1029/2006JC003901

Fay, A. R., & McKinley, G. A. (2014). Global open-ocean biomes: Mean and temporal variability. *Earth System Science Data*, *6*(2), 273–284. https://doi.org/10.5194/essd-6-273-2014

Fernandes. (2014). *python-seawater v3.3.2*. https://doi.org/10.5281/ZENODO.11395

Fox, J., Behrenfeld, M. J., Haëntjens, N., Chase, A., Kramer, S. J., Boss, E., Karp-Boss, L., Fisher, N. L., Penta, W. B., Westberry, T. K., & Halsey, K. H. (2020). Phytoplankton Growth and Productivity in the Western North Atlantic: Observations of Regional Variability From the NAAMES Field Campaigns. *Frontiers in Marine Science*, *7*, 24. https://doi.org/10.3389/FMARS.2020.00024/BIBTEX

Galí, M., Devred, E., Babin, M., & Levasseur, M. (2019). Decadal increase in Arctic dimethylsulfide emission. *Proceedings of the National Academy of Sciences of the United States of America*, *116*(39), 19311–19317. https://doi.org/10.1073/PNAS.1904378116/-/DCSUPPLEMENTAL

Galí, M., Devred, E., Levasseur, M., Royer, S. J., & Babin, M. (2015). A remote sensing algorithm for planktonic dimethylsulfoniopropionate (DMSP) and an analysis of global patterns. *Remote Sensing of Environment*, *171*, 171–184. https://doi.org/10.1016/j.rse.2015.10.012

Galí, M., Levasseur, M., Devred, E., Simó, R., & Babin, M. (2018). Sea-surface dimethylsulfide (DMS) concentration from satellite data at global and regional scales. *Biogeosciences*, *15*(11), 3497–3519. https://doi.org/10.5194/bg-15-3497-2018

Galí, M., Lizotte, M., Kieber, D. J., Randelhoff, A., Hussherr, R., Xue, L., Dinasquet, J., Babin, M., Rehm, E., & Levasseur, M. (2021). DMS emissions from the Arctic marginal ice zone. *Elementa: Science of the Anthropocene*, *9*(1). https://doi.org/10.1525/ELEMENTA.2020.00113

Galí, M., & Simó, R. (2015). A meta-analysis of oceanic DMS and DMSP cycling processes: Disentangling the summer paradox. *Global Biogeochemical Cycles*, *29*(4), 496–515. https://doi.org/10.1002/2014GB004940

Gaube, P., J. McGillicuddy, D., & Moulin, A. J. (2019). Mesoscale Eddies Modulate Mixed Layer Depth Globally. *Geophysical Research Letters*, *46*(3), 1505–1512. https://doi.org/10.1029/2018GL080006

535   Hales, B., & Takahashi, T. (2004). High-resolution biogeochemical investigation of the Ross Sea, Antarctica, during the AESOPS (U. S. JGOFS) Program. *Global Biogeochemical Cycles*, *18*(3). https://doi.org/10.1029/2003GB002165

Halloran, P. R., Bell, T. G., & Totterdell, I. J. (2010). Can we trust empirical marine DMS parameterisations within projections of future climate? *Biogeosciences*, *7*(5), 1645–1656. https://doi.org/10.5194/bg-7-1645-2010

Herr, A. E., Kiene, R. P., Dacey, J. W. H., & Tortell, P. D. (2019). Patterns and drivers of dimethylsulfide concentration in the
540   northeast subarctic Pacific across multiple spatial and temporal scales. *Biogeosciences*, *16*, 1729–1754. https://doi.org/10.5194/bg-16-1729-2019

Hulswar, S., Simó, R., Galí, M., Bell, T. G., Lana, A., Inamdar, S., Halloran, P. R., Manville, G., & Mahajan, A. S. (2022). Third revision of the global surface seawater dimethyl sulfide climatology (DMS-Rev3). *Earth System Science Data*, *14*(7), 2963–2987. https://doi.org/10.5194/essd-14-2963-2022

545   Humphries, G. R. W., Deal, C. J., Elliott, S., & Huettmann, F. (2012). Spatial predictions of sea surface dimethylsulfide concentrations in the high arctic. *Biogeochemistry*, *110*(1–3), 287–301. https://doi.org/10.1007/S10533-011-9683-Y/FIGURES/7

Jacobs, G. A., Barron, C. N., & Rhodes, R. C. (2001). Mesoscale characteristics. *JOURNAL OF GEOPHYSICAL RESEARCH*, *106*(C9), 581–600. https://doi.org/10.1029/2000JC000669

550   Kettle, A. J., Andreae, M. O., Amouroux, D., Andreae, T. W., Bates, T. S., Berresheim, H., Bingemer, H., Boniforti, R., Curran, M. A. J., DiTullio, G. R., Helas, G., Jones, G. B., Keller, M. D., Kiene, R. P., Leek, C., Levasseur, M., Malin, G., Maspero, M., Matrai, P., … Uher, G. (1999). A global database of sea surface dimethylsulfide (DMS) measurements and a procedure to predict sea surface DMS as a function of latitude, longitude, and month. *Global Biogeochemical Cycles*, *13*(2), 399–444. https://doi.org/10.1029/1999GB900004

555   Klocker, A., Marshall, D. P., Keating, S. R., & Read, P. L. (2016). A regime diagram for ocean geostrophic turbulence. *Quarterly Journal of the Royal Meteorological Society Q. J. R. Meteorol. Soc*, *142*, 2411–2417. https://doi.org/10.1002/qj.2833

Lana, A., Bell, T. G., Simó, R., Vallina, S. M., Ballabrera-Poy, J., Kettle, A. J., Dachs, J., Bopp, L., Saltzman, E. S., Stefels, J., Johnson, J. E., & Liss, P. S. (2011). An updated climatology of surface dimethlysulfide concentrations and emission
560   fluxes in the global ocean. *Global Biogeochemical Cycles*, *25*(1), 1–17. https://doi.org/10.1029/2010GB003850

Lannuzel, D., Tedesco, L., van Leeuwe, M., Campbell, K., Flores, H., Delille, B., Miller, L., Stefels, J., Assmy, P., Bowman, J., Brown, K., Castellani, G., Chierici, M., Crabeck, O., Damm, E., Else, B., Fransson, A., Fripiat, F., Geilfus, N. X., … Wongpan, P. (2020). The future of Arctic sea-ice biogeochemistry and ice-associated ecosystems. *Nature Climate Change 2020 10:11*, *10*(11), 983–992. https://doi.org/10.1038/s41558-020-00940-4

Mahajan, A. S., Fadnavis, S., Thomas, M. A., Pozzoli, L., Gupta, S., Royer, S. J., Saiz-Lopez, A., & Simó, R. (2015). Quantifying the impacts of an updated global dimethyl sulfide climatology on cloud microphysics and aerosol radiative forcing. *Journal of Geophysical Research*, *120*(6), 2524–2536. https://doi.org/10.1002/2014JD022687

McGillicuddy, D. J. (2016). Mechanisms of Physical-Biological-Biogeochemical Interaction at the Oceanic Mesoscale. *Http://Dx.Doi.Org/10.1146/Annurev-Marine-010814-015606*, *8*, 125–159. https://doi.org/10.1146/ANNUREV-MARINE-010814-015606

McNabb, B. J., & Tortell, P. D. (2022). Improved prediction of dimethyl sulfide (DMS) distributions in the northeast subarctic Pacific using machine-learning algorithms. *Biogeosciences*, *19*(6), 1705–1721. https://doi.org/10.5194/BG-19-1705-2022

McNabb, B. J., & Tortell, P. D. (2023). Oceanographic controls on Southern Ocean dimethyl sulfide distributions revealed by machine learning algorithms. *Limnology and Oceanography*. https://doi.org/10.1002/LNO.12298

Miles, C. J., Bell, T. G., & Lenton, T. M. (2009). Testing the relationship between the solar radiation dose and surface DMS concentrations using in situ data. *Biogeosciences*, *6*, 1927–1934. www.biogeosciences.net/6/1927/2009/

Mulcahy, J. P., Johnson, C., Jones, C. G., Povey, A. C., Scott, C. E., Sellar, A., Turnock, S. T., Woodhouse, M. T., Abraham, N. L., Andrews, M. B., Bellouin, N., Browse, J., Carslaw, K. S., Dalvi, M., Folberth, G. A., Glover, M., Grosvenor, D. P., Hardacre, C., Hill, R., … Yool, A. (2020). Description and evaluation of aerosol in UKESM1 and HadGEM3-GC3.1 CMIP6 historical simulations. *Geoscientific Model Development*, *13*(12), 6383–6423. https://doi.org/10.5194/GMD-13-6383-2020

NASA Goddard Space Flight Center, O. E. L. O. B. P. Group. (2018). *Moderate-resolution Imaging Spectroradiometer (MODIS) Aqua Chlorophyll Data; 2018 Reprocessing*. NASA OB.DAAC, Greenbelt, MD, USA. https://doi.org/10.5067/AQUA/MODIS/L3M/CHL/2018

Nemcek, N., Ianson, D., & Tortell, P. D. (2008). A high-resolution survey of DMS, CO2, and O2/Ar distributions in productive coastal waters. *Global Biogeochemical Cycles*, *22*(2). https://doi.org/10.1029/2006GB002879

Nowinski, B., Motard-Côté, J., Landa, M., Preston, C. M., Scholin, C. A., Birch, J. M., Kiene, R. P., & Moran, M. A. (2019). Microdiversity and temporal dynamics of marine bacterial dimethylsulfoniopropionate genes. *Environmental Microbiology*, *21*(5), 1687–1701. https://doi.org/10.1111/1462-2920.14560

Polimene, L., Archer, S. D., Butenschön, M., & Allen, J. I. (2012). A mechanistic explanation of the Sargasso Sea DMS "summer paradox." *Biogeochemistry*, *110*(1), 243–255. https://doi.org/10.1007/s10533-011-9674-z

Quinn, P. K., Coffman, D. J., Johnson, J. E., Upchurch, L. M., & Bates, T. S. (2017). Small fraction of marine cloud condensation nuclei made up of sea spray aerosol. *Nature Geoscience 2017 10:9*, *10*(9), 674–679. https://doi.org/10.1038/ngeo3003

Rhines, P. B. (1975). Waves and turbulence on a beta-plane. *J. Fluid Mech*, *69*, 417–443. https://doi.org/10.1017/S0022112075001504

Royer, S. J., Galí, M., Mahajan, A. S., Ross, O. N., Pérez, G. L., Saltzman, E. S., & Simó, R. (2016). A high-resolution time-depth view of dimethylsulphide cycling in the surface sea. *Scientific Reports*, *6*. https://doi.org/10.1038/srep32325

Royer, S. J., Mahajan, A. S., Galí, M., Saltzman, E., & Simõ, R. (2015). Small-scale variability patterns of DMS and phytoplankton in surface waters of the tropical and subtropical Atlantic, Indian, and Pacific Oceans. *Geophysical Research Letters*, *42*(2), 475–483. https://doi.org/10.1002/2014GL062543

Saltzman, E. S., de Bruyn, W. J., Lawler, M. J., Marandino, C. A., & McCormick, C. A. (2009). A chemical ionization mass spectrometer for continuous underway shipboard analysis of dimethylsulfide in near-surface seawater. *Ocean Science*, *5*(4), 537–546. https://doi.org/10.5194/os-5-537-2009

Sanchez, K. J., Chen, C. L., Russell, L. M., Betha, R., Liu, J., Price, D. J., Massoli, P., Ziemba, L. D., Crosbie, E. C., Moore, R. H., Müller, M., Schiller, S. A., Wisthaler, A., Lee, A. K. Y., Quinn, P. K., Bates, T. S., Porter, J., Bell, T. G., Saltzman, E. S., … Behrenfeld, M. J. (2018). Substantial Seasonal Contribution of Observed Biogenic Sulfate Particles to Cloud Condensation Nuclei. *Scientific Reports 2018 8:1*, *8*(1), 1–14. https://doi.org/10.1038/s41598-018-21590-9

Scott, R. B., & Wang, F. (2005). Direct Evidence of an Oceanic Inverse Kinetic Energy Cascade from Satellite Altimetry. *Journal of Physical Oceanography*, *35*(9), 1650–1666. https://doi.org/10.1175/JPO2771.1

Simó, R. (2001). Production of atmospheric sulfur by oceanic plankton: biogeochemical, ecological and evolutionary links. *Trends in Ecology & Evolution*, *16*(6), 287–294. http://tree.trends.com

Simó, R., & Dachs, J. (2002). Global ocean emission of dimethylsulfide predicted from biogeophysical data. *Global Biogeochemical Cycles*, *16*(4), 26-1-26–10. https://doi.org/10.1029/2001GB001829

Simó, R., Saló, V., Almeda, R., Movilla, J., Trepat, I., Saiz, E., & Calbet, A. (2018). The quantitative role of microzooplankton grazing in dimethylsulfide (DMS) production in the NW Mediterranean. *Biogeochemistry*, *141*(2), 125–142. https://doi.org/10.1007/S10533-018-0506-2/TABLES/3

Stefels, J., van Leeuwe, M. A., Jones, E. M., Meredith, M. P., Venables, H. J., Webb, A. L., & Henley, S. F. (2018). Impact of sea-ice melt on dimethyl sulfide (sulfoniopropionate) inventories in surface waters of Marguerite Bay, West Antarctic Peninsula. *Philosophical Transactions of the Royal Society A: Mathematical, Physical and Engineering Sciences*, *376*(2122). https://doi.org/10.1098/RSTA.2017.0169

Tesdal, J.-E., Christian, J. R., Monahan, A. H., Salzen, K. von, Tesdal, J.-E., Christian, J. R., Monahan, A. H., & Salzen, K. von. (2015). Evaluation of diverse approaches for estimating sea-surface DMS concentration and air–sea exchange at global scale. *Environmental Chemistry*, *13*(2), 390–412. https://doi.org/10.1071/EN14255

Toole, D. A., & Siegel, D. A. (2004). Light-driven cycling of dimethylsulfide (DMS) in the Sargasso Sea: Closing the loop. *Geophysical Research Letters*, *31*(9). https://doi.org/https://doi.org/10.1029/2004GL019581

Toole, D. A., Siegel, D. A., & Doney, S. C. (2008). A light-driven, one-dimensional dimethylsulfide biogeochemical cycling model for the Sargasso Sea. *Journal of Geophysical Research: Biogeosciences*, *113*(G2). https://doi.org/https://doi.org/10.1029/2007JG000426

Tortell, P. D. (2005a). Dissolved gas measurements in oceanic waters made by membrane inlet mass spectrometry. *Limnology and Oceanography: Methods*, *3*(1), 24–37. https://doi.org/10.4319/lom.2005.3.24

Tortell, P. D. (2005b). Small-scale heterogeneity of dissolved gas concentrations in marine continental shelf waters. *Geochemistry, Geophysics, Geosystems*, *6*(11). https://doi.org/10.1029/2005GC000953

635   Tortell, P. D., Guéguen, C., Long, M. C., Payne, C. D., Lee, P., & DiTullio, G. R. (2011). Spatial variability and temporal dynamics of surface water pCO2, δO2/Ar and dimethylsulfide in the Ross Sea, Antarctica. *Deep-Sea Research Part I: Oceanographic Research Papers*, *58*(3), 241–259. https://doi.org/10.1016/j.dsr.2010.12.006

Tortell, P. D., & Long, M. C. (2009). Spatial and temporal variability of biogenic gases during the Southern Ocean spring bloom. *Geophysical Research Letters*, *36*(1). https://doi.org/10.1029/2008GL035819

640   Tulloch, R., Marshall, J., Hill, C., & Smith, K. S. (2011). Scales, Growth Rates, and Spectral Fluxes of Baroclinic Instability in the Ocean. *Journal of Physical Oceanography*, *41*(6), 1057–1076. https://doi.org/10.1175/2011JPO4404.1

Vallina, S. M., & Simó, R. (2007). Strong Relationship Between DMS and the Solar Radiation Dose over the Global Surface Ocean. *Science (New York, N.Y.)*, *315*(5811), 506–508. https://doi.org/10.1126/science.281.5374.200

Vallina, S. M., Simó, R., Anderson, T. R., Gabric, A., Cropp, R., & Pacheco, J. M. (2008). A dynamic model of oceanic sulfur

645   (DMOS) applied to the Sargasso Sea: Simulating the dimethylsulfide (DMS) summer paradox. *Journal of Geophysical Research: Biogeosciences*, *113*(1). https://doi.org/10.1029/2007JG000415

Wang, W.-L., Song, G., Primeau, F., Saltzman, E. S., Bell, T. G., & Moore, J. K. (2020). Global ocean dimethyl sulfide climatology estimated from observations and an artificial neural network. *Biogeosciences*, *17*, 5335–5354. https://doi.org/10.5194/bg-17-5335-2020

650   Williams, R. G., & Follows, M. J. (2011). Ocean eddies. In *Ocean Dynamics and the Carbon Cycle* (pp. 211–235). Cambridge University Press. https://doi.org/10.1017/CBO9780511977817.010

Woodhouse, M. T., Carslaw, K. S., Mann, G. W., Vallina, S. M., Vogt, M., Halloran, P. R., & Boucher, O. (2010). Low sensitivity of cloud condensation nuclei to changes in the sea-air flux of dimethyl-sulphide. *Atmospheric Chemistry and Physics*, *10*(16), 7545–7559. https://doi.org/10.5194/acp-10-7545-2010

655   Woodhouse, M. T., Mann, G. W., Carslaw, K. S., & Boucher, O. (2013). Sensitivity of cloud condensation nuclei to regional changes in dimethyl-sulphide emissions. *Atmospheric Chemistry and Physics*, *13*(5), 2723–2733. https://doi.org/10.5194/acp-13-2723-2013

Zindler, C., Marandino, C. A., Bange, H. W., Schütte, F., & Saltzman, E. S. (2014). Nutrient availability determines dimethyl sulfide and isoprene distribution in the eastern Atlantic Ocean. *Geophysical Research Letters*, *41*(9), 3181–3188.

660   https://doi.org/10.1002/2014GL059547

Zlotnicki, V., Qu, Z., & Willis, J. (2019). *MEaSUREs Gridded Sea Surface Height Anomalies Version 1812 | PO.DAAC / JPL / NASA*. https://podaac.jpl.nasa.gov/dataset/SEA_SURFACE_HEIGHT_ALT_GRIDS_L4_2SATS_5DAY_6THDEG_V_JPL1 812

665
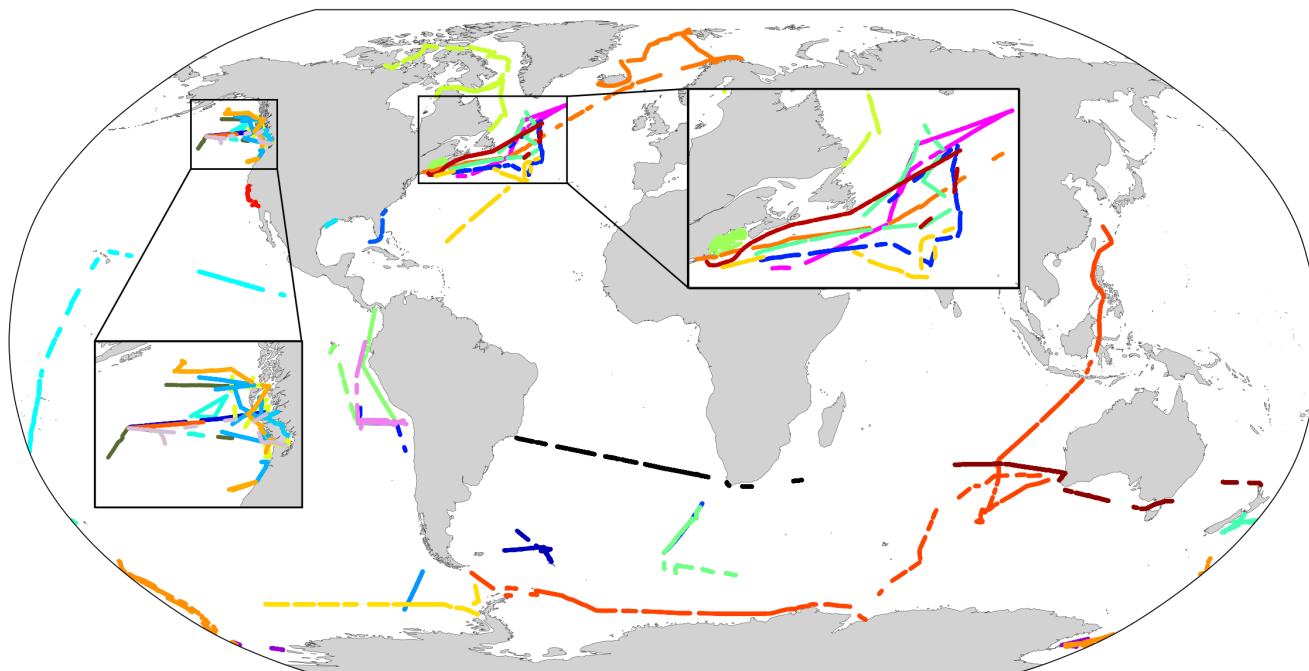
Figure 1: Global extent of the 37 high frequency DMS campaigns included in this analysis (coloured). Data are only shown for the underway transects used in the VLS analysis (see Sect. 2.3). Insets show detail for northeast Pacific and northwest Atlantic regions with multiple sampling campaigns (see Table S2 and Fig. S1 in the Supplementary Material for metadata relating to each sampling campaign and the spatiotemporal distribution, respectively).
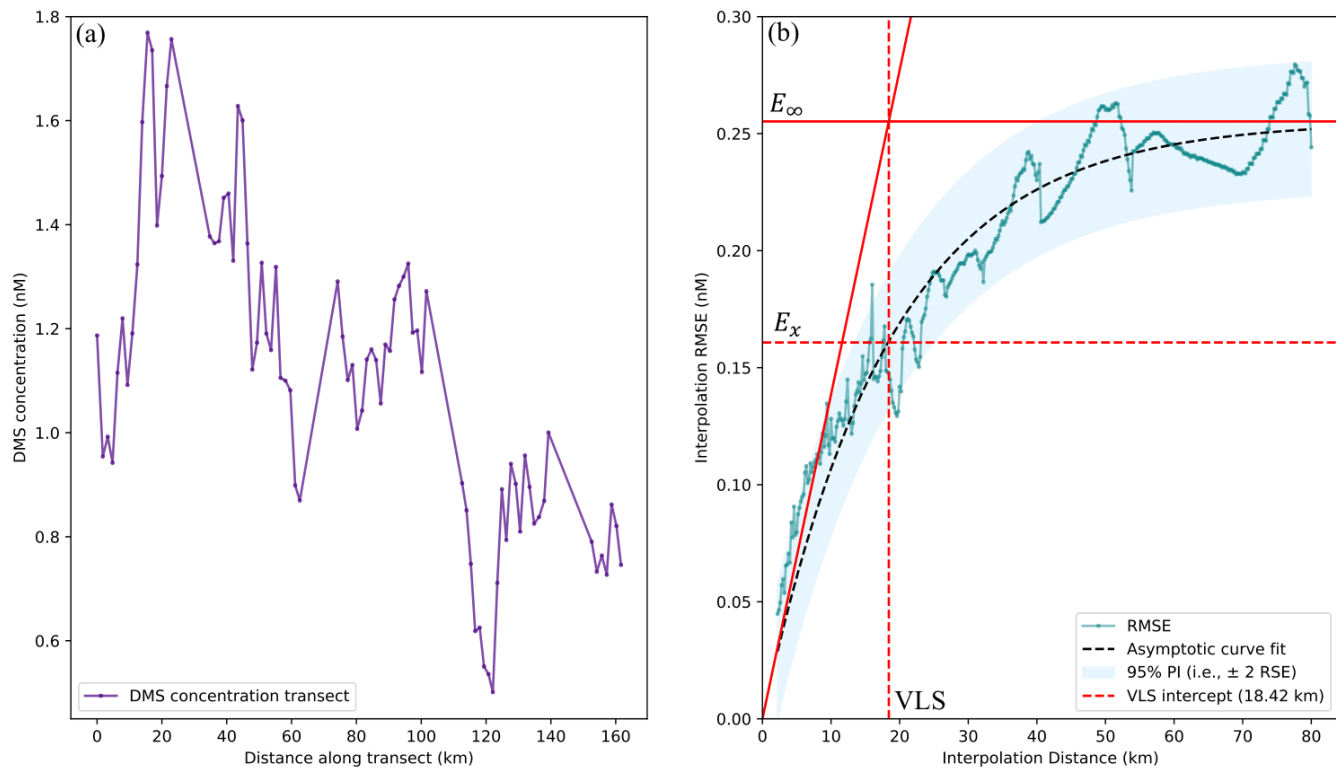
Figure 2: (a) Example seawater DMS concentration (nM) data transect (sampled from the northwest Atlantic during the NAAMES1 (November 2015) campaign; see Bell et al., 2021), analysed to find the variability lengthscale (VLS). (b) Asymptotic error curve (dashed black) fitted to interpolation errors (RMSE, nM; dotted cyan) plotted as a function of increasingly coarse interpolation distance (km). The 95% prediction intervals (PI) of the non-linear regression fit, i.e., $\pm\, 2 \times$ residual standard errors (RSE), are shaded blue. The VLS (km) is characterised as the intercept (dashed red) on the curve at 63% of the asymptotically approached maximum interpolation error (nM). Method adapted from Hales & Takahashi (2004).

675
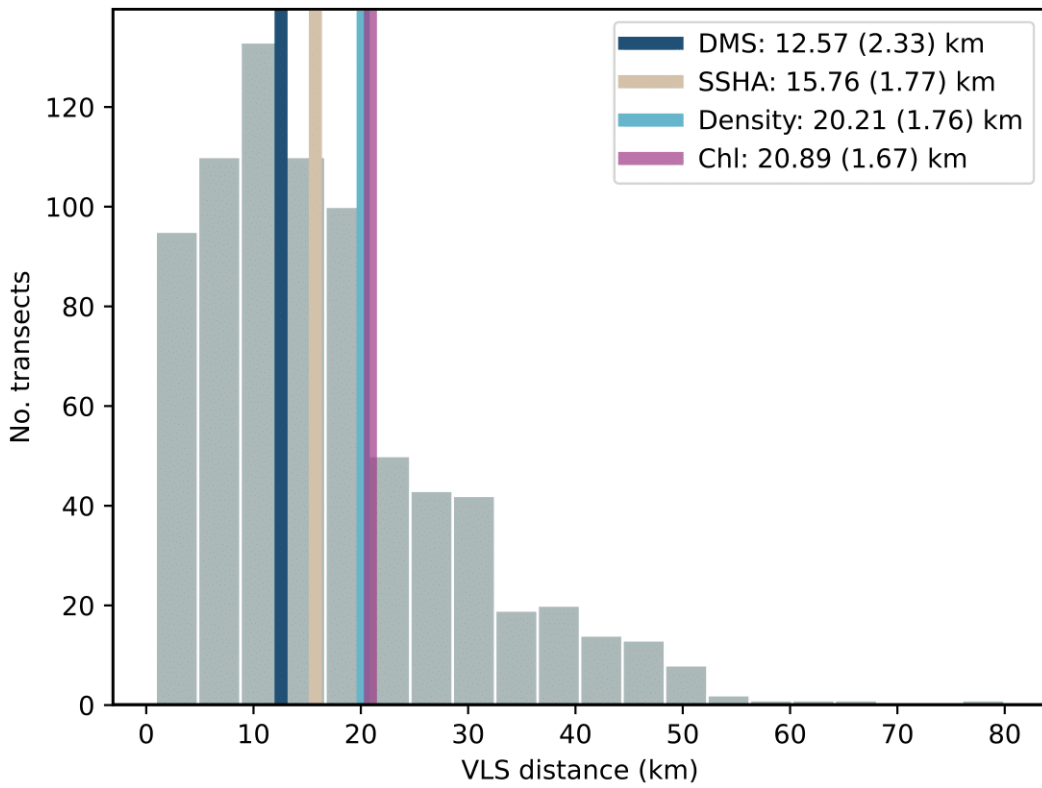
680

Figure 3: Frequency distribution of variability lengthscales (VLS, km) for all DMS transects (grey bars). Vertical coloured lines correspond to the global geometric mean (and geometric standard deviation, GSD) from all transects for VLS$_{DMS}$ (dark blue), VLS$_{SSHA}$ (beige), VLS$_{density}$ (cyan), VLS$_{Chl}$ (magenta).

685
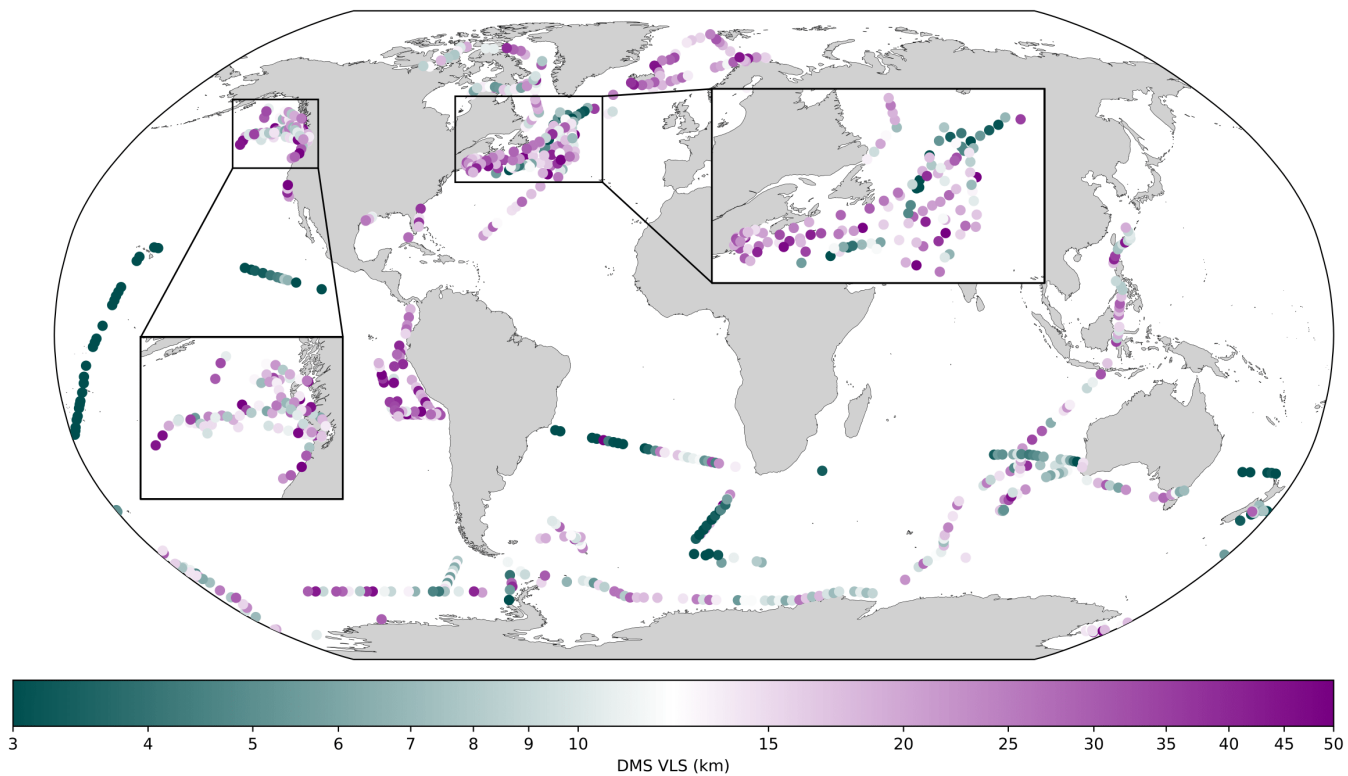
Figure 4: Global distribution of 763 transects coloured by VLS$_{DMS}$ (km, log scale). The colour bar diverges at the global geometric mean VLS$_{DMS}$ (12.57 km). See Fig. S3 in the Supplementary Material for equivalent VLS distribution maps of Chl, density, SSHA, salinity and SST, and Fig. S1 for the spatiotemporal distribution of VLS$_{DMS}$.

690
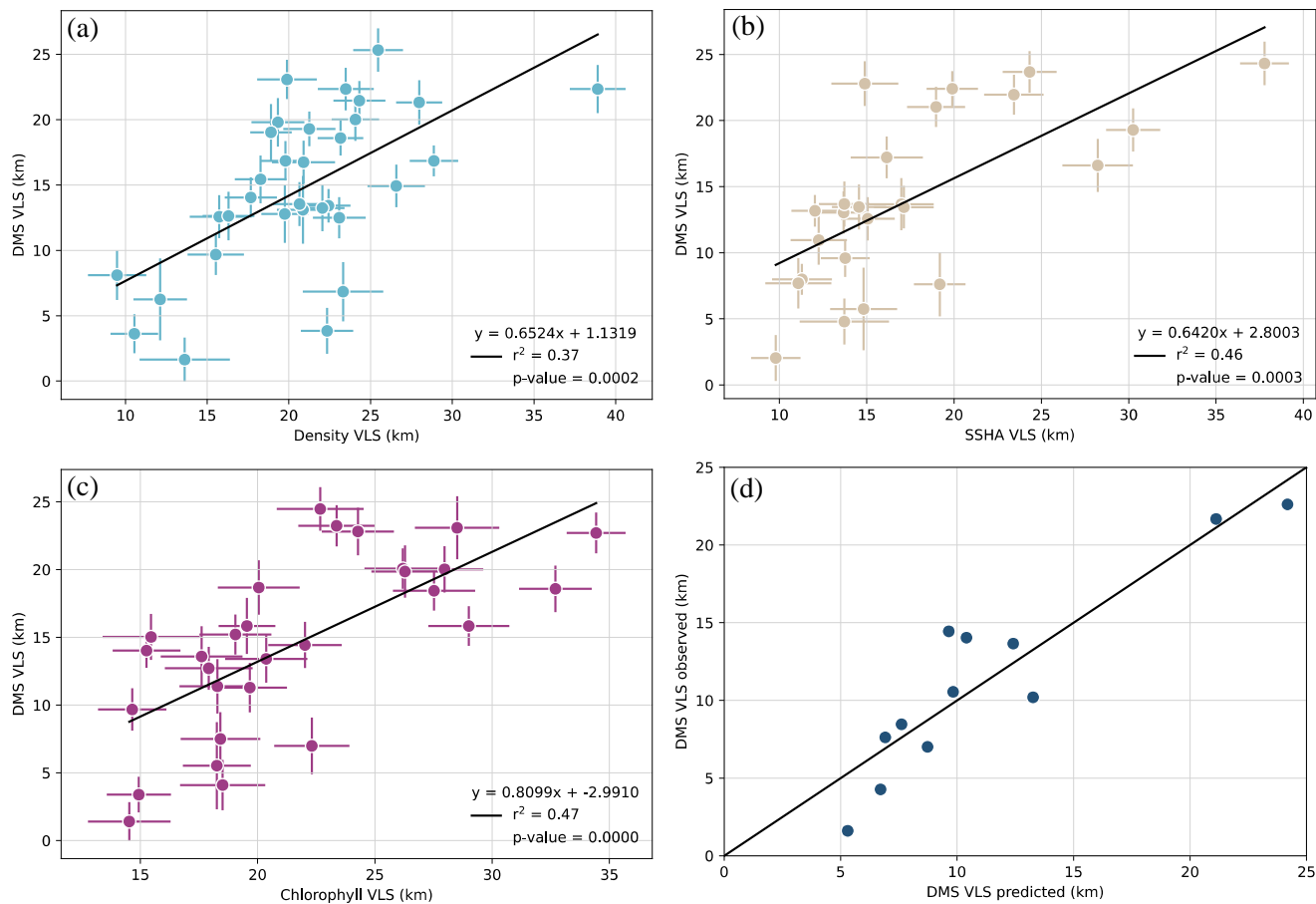
Figure 5: Campaign geometric mean VLS$_{DMS}$ (km) plotted versus (a) VLS$_{density}$, (b) VLS$_{SSHA}$, and (c) VLS$_{Chl}$. Error bars indicate 1 GSD of the data within each campaign. (d) Campaign geometric mean VLS$_{DMS}$ predicted using coefficients from the VLS$_{SSHA-Chl-Density}$ multiple linear regression model (Model 7, Table 1; Supplementary Material, Table S4; Fig. S4) versus observed VLS$_{DMS}$, for the subset of 12 DMS campaigns included in the multiple linear regression model. The 1:1 line is shown.

695

700

705

Table 1: Regression results for the prediction of campaign average VLS$_{DMS}$, using different combinations of input parameters. Models are ranked in order of how much VLS$_{DMS}$ variance is explained. Models that are significant ($p < 0.01$) are denoted using *.

Model no.	Input parameters	R^2	Adj. R^2	p	Relative importance (%)	N (no. of campaigns)	No. transects used to calculate campaign averages (of 760)
Linear Regression							
1	VLS$_{Chl}$	0.47	–	<0.01*	100	29	351
2	VLS$_{SSHA}$	0.46	–	<0.01*	100	24	361
3	VLS$_{density}$	0.37	–	<0.01*	100	32	480
4	VLS$_{salinity}$	0.33	–	<0.01*	100	32	490
5	VLS$_{SST}$	0.21	–	0.014	100	28	445
6	Latitude (abs.)	0.02	–	0.375	100	35	760
Multiple Linear Regression							
7	VLS$_{Chl}$ VLS$_{SSHA}$ VLS$_{density}$	0.83	0.77	<0.01*	34 52 14	12	87
8	VLS$_{Chl}$ VLS$_{SSHA}$ VLS$_{salinity}$	0.77	0.71	<0.01*	58 41 1	15	100
9	VLS$_{Chl}$ VLS$_{density}$	0.66	0.63	<0.01*	54 46	26	224
10	VLS$_{salinity}$ VLS$_{SST}$	0.62	0.59	<0.01*	85 15	25	322
11	VLS$_{Chl}$ VLS$_{SSHA}$	0.51	0.46	<0.01*	35 65	20	177
12	VLS$_{Chl}$ VLS$_{salinity}$	0.50	0.45	<0.01*	70 30	22	211
13	VLS$_{SSHA}$ VLS$_{salinity}$	0.49	0.44	<0.01*	91 9	23	234
14	VLS$_{Chl}$ VLS$_{SST}$	0.46	0.4	<0.01*	73 27	22	204
15	VLS$_{SSHA}$ VLS$_{SST}$	0.43	0.36	<0.01*	75 25	20	189
16	VLS$_{SSHA}$ VLS$_{density}$	0.41	0.35	<0.01*	84 16	22	213
17	VLS$_{Chl}$ VLS$_{SSHA}$ VLS$_{SST}$	0.50	0.29	0.156	84 15 1	11	77